Effect of Folate-Targeted Nanoparticle Size on Their Rates of Penetration into Solid Tumors

Erina Vlashi,[†,§] Lindsay E. Kelderhouse,[†] Jennifer E. Sturgis,[‡] and Philip S. Low[†,*]

[†]Department of Chemistry, Purdue University, West Lafayette, Indiana 47907, United States and [‡]Department of Basic Medical Sciences, Purdue University, West Lafayette, Indiana 47907, United States. [§]Present address: Department of Radiation Oncology, David Geffen School of Medicine at UCLA, 10833 Le Conte Ave, Los Angeles, California 90095-1714, United States.

ABSTRACT Targeted therapies are emerging as a preferred strategy for the treatment of cancer and other diseases. To evaluate the impact of a high affinity targeting ligand on the rate and extent of tumor penetration of different sized nanomedicines, we have used intravital multiphoton microscopy to quantitate the kinetics of tumor accumulation of a homologous series of folate-PEG-rhodamine conjugates prepared with polyethylene glycols (PEG) of different molecular weights. We demonstrate that increasing the size of the folate-PEG-rhodamine conjugates results in both longer circulation times and slower tumor penetration rates. Although a "binding site barrier" is observed with the folate-linked polymers in folate receptor expressing tumors, ligand targeting eventually leads to increased tumor accumulation, with endocytosis of the targeted nanocarriers contributing to their enhanced tumor retention. Because the effects of nanocarrier size, shape, chemistry, and targeting ligand are interconnected and complex, we suggest that these parameters must be carefully optimized for each nanocarrier to ensure optimal drug delivery *in vivo*.

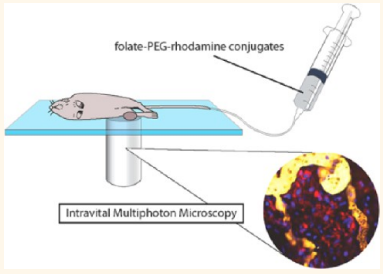

KEYWORDS: folate receptor · tumor accumulation · nanomedicines size · intravital multiphoton microscopy · binding site barrier

Nanomedicines (*e.g.*, liposomes, biocompatible copolymers, dendrimers, inorganic nanoparticles, viral vectors, micelles, aptamers, protein aggregates, and antibodies, *etc.*) have attracted significant attention in recent years due to their large drug carrying capacity, passive accumulation in malignant and inflamed tissues, long circulation times, and adaptability to multiple functions.[1−16] While such desirable attributes have been frequently applauded, concerns regarding the efficiency of nanomedicine extravasation and perfusion through interstitial spaces to malignant targets have also arisen.[17,18] Tumor penetration concerns have been especially heightened by observations that a positive interstitial hydrostatic pressure may exist within malignant masses that suppresses convective flow from proximal blood vessels into the tumor core.[19,20]

Although use of targeting ligands to enhance uptake of nanoparticles by pathologic cells has recently increased,[21−31] almost nothing is known regarding the impact of high affinity targeting ligands on the rate and extent of nanoparticle tumor penetration. A "binding site barrier" has been postulated by Weinstein and co-workers, where the first few targeted macromolecules to escape a blood vessel are predicted to bind to proximal cancer cells and obstruct passage of subsequent macromolecules to deeper sites within the tumor.[32−35] Our lab has, in fact, demonstrated that a low molecular weight folate-targeted drug experiences a mild and transient "binding site barrier"; however, this brief delay in tumor penetration is followed by efficient perfusion of the drug throughout the tumor mass, resulting in no permanent deficiency in tumor delivery.[36]

To begin to address the impact of a high affinity targeting ligand on the rate and depth of penetration of various sized nanomedicines into solid tumors, we have designed a model system comprised of a targeting ligand linked to a polymer of the desired size and a fluorescent dye for use in *in vivo* visualization. Folic acid was selected for tumor-specific targeting, because its receptor (FR) is overexpressed on a large

* Address correspondence to plow@purdue.edu.

Received for review May 24, 2013 and accepted September 10, 2013.

Published online September 10, 2013
10.1021/nn402644g

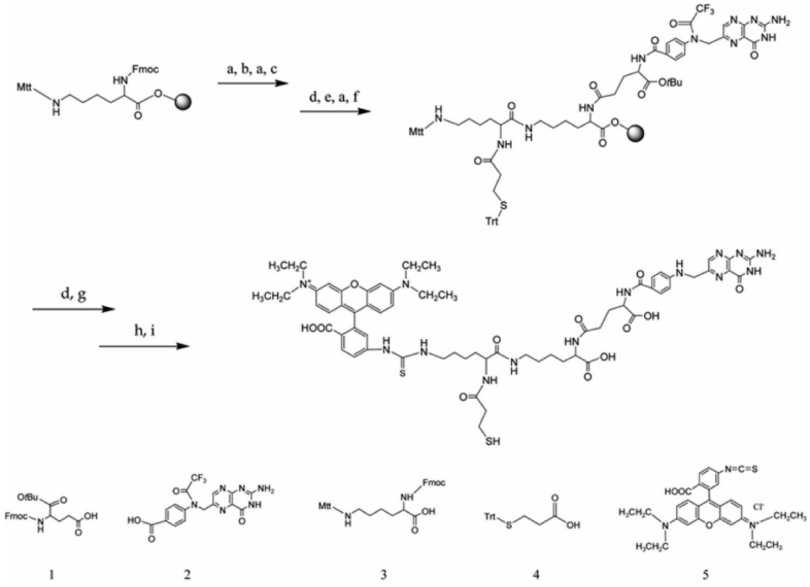

Scheme 1. Synthesis of folate-rhodamine-SH "anchor". Reagents and conditions: (a) 20% piperidine in DMF, (b) Fmoc-Glu-OtBu(1)/HOBt/HBTU/DIPEA/DMF, (c) Pteroic acid(2)/ HOBt/HBTU/DIPEA/DMF, (d) 1% TFA/DCM, (e) Fmoc-Lys(Mtt)−OH(3)/HOBT/HBTU/DIPEA/DMF, (f) *S*-Trityl-3-mercaptopropionic acid(4)/HOBT/HBTU/DIPEA/DMF, (g) Rhodamine B isothiocyanate-(5)/DIPEA, (h) 94.5% TFA/2.5% H_2O/1% triisopropylsilane, (i) $NH4^+OH$, pH 10.

fraction of human cancers,[37−39] and since it binds FR with high affinity (K_d ~10^{-9} M). Polyethylene glycol (PEG) polymers of different molecular weights were chosen to mimic different sized nanomedicines, since (1) they are commercially available in different molecular weights that allow investigation of the impact of nanoparticle size without interference from variations in particle charge or surface chemistry, (2) they can all be conjugated to a single folic acid with the same chemistry, thereby avoiding artifacts arising from multivalent interactions, and (3) they are highly water-soluble, facilitating their distribution throughout the vascularized tissues of live animals. Finally, a single rhodamine B fluorophore was conjugated to each folate-PEG construct to enable visualization and quantitation of the rates of conjugate penetration throughout solid tumor masses *in vivo*.

RESULTS AND DISCUSSION

Synthesis and Characterization of Folate-PEG-Rhodamine Conjugates of Various Molecular Weights. A series of tumor-targeted fluorescent conjugates, linked to different sized polyethylene glycol (PEG) polymers, were synthesized with a common folate-rhodamine "anchor" for the purpose of comparing their pharmacokinetics of tumor extravasation and perfusion. As shown in Scheme 1, folic acid was first linked to the α-amino group of lysine *via* standard solid phase chemistry, after which a second lysine was tethered to the ε-amino group of the first lysine. After deprotection of the second lysine's α-amino group and ligation of the same amine to mercaptopropionic acid, the ε-amino group of the second lysine was conjugated to rhodamine, leaving a protected thiol for subsequent attachment to the desired maleimide-derivatized PEG (Scheme 2). Following purification, each folate-PEG-rhodamine conjugate was analyzed for (1) apparent molecular weight, (2) folate to rhodamine ratio, (3) fluorescence intensity, and (4) affinity and specificity for the folate receptor (FR). The apparent molecular weight of each conjugate was determined by monitoring its retention time on a gel filtration column. As seen in Figure 1, in all cases, the elution volume of the folate-targeted PEG conjugate was similar to the elution volume of the unconjugated PEG, demonstrating that attachment of neither folate nor rhodamine affected the apparent size of the conjugate (compare red and blue circles). More importantly, the apparent molecular weights of all PEG molecules and their folate-rhodamine conjugates were ~8 times larger than their true molecular weights, with folate-PEG(5 000)-rhodamine eluting from the gel filtration column at an apparent M_r ~30 000 Da, and folate-PEG(20 000)-rhodamine and folate-PEG(60 000)-rhodamine eluting with apparent M_r ~200 000 and ~450 000 Da, respectively. These unusually large hydrodynamic radii of PEG polymers, which have been previously reported,[42] render their folate conjugates useful models for study of the penetration of targeted nanomedicines of various sizes into solid tumors.

The ratio of folate to rhodamine was next analyzed by measuring the absorbance of folate and rhodamine for each conjugate at 280 and 560 nm, respectively, after which the molar ratio of folate to rhodamine was calculated as described in Supporting Information Figure S2. This ratio was expected to be 1:1 on the basis of the stoichiometry of conjugate synthesis (Scheme 1), and this expectation was confirmed in all

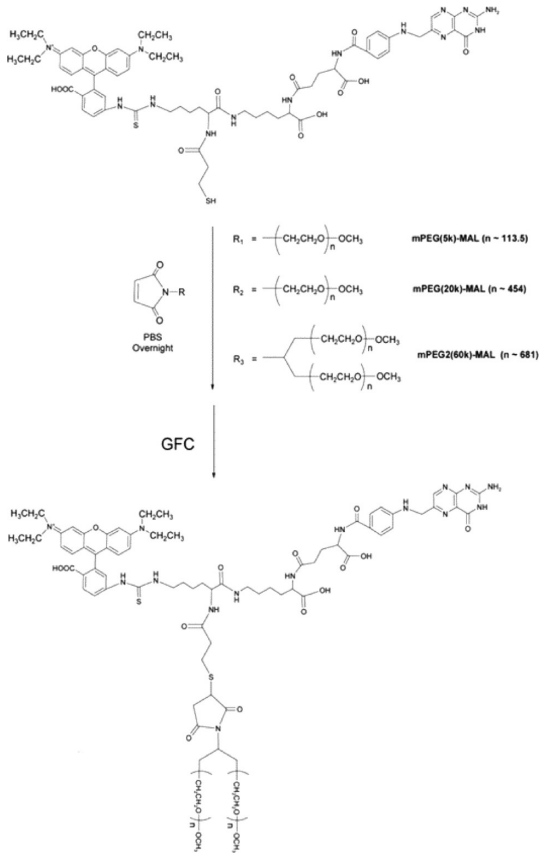

Scheme 2. Method for attachment of PEG-maleimide molecules of different sizes to the folate-rhodamine "anchor". Maleimide-activated PEG molecules were dissolved in PBS and added to a 5-fold molar excess of folate-rhodamine-SH with stirring overnight at room temperature under nitrogen. Compounds were purified by gel filtration chromatography (GFC) as described in the Materials and Methods.

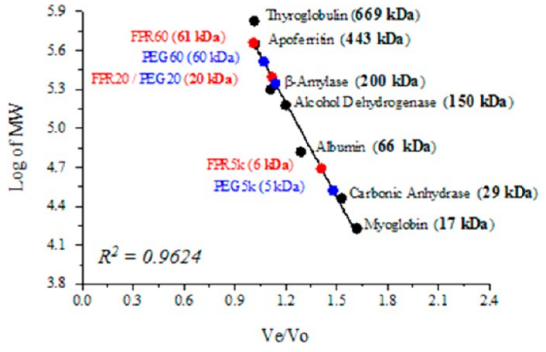

Figure 1. Characterization of folate-PEG-rhodamine conjugates by size exclusion chromatography. Folate-PEG-rhodamine conjugates dissolved in PBS were separated by size exclusion chromatography on Sephacryl 100-HR and 200-HR columns. Black circles: standard curve for the apparent molecular weight markers, as indicated; red circles: folate-PEG-rhodamine conjugates (folate-PEG(5000)-rhodamine[FPR5k], folate-PEG(20 000)-rhodamine [FPR20k], folate-PEG(60 000) [FRP60k]); blue circles: nontargeted PEG molecule of the same molecular weights.

cases, suggesting that all conjugates have a folate and a rhodamine. Confirmation of this stoichiometry was important to ensure that penetration of folate-PEG-rhodamine conjugates into tumors was not impacted by large quantities of "invisible" folate-PEG conjugates or "nonbinding" PEG-rhodamine conjugates.

Third, it was important to confirm that addition of the PEG moiety to the folate-rhodamine backbone did not quench rhodamine fluorescence. For this purpose, the fluorescence intensity of each conjugate was examined at the same concentration and shown to be nearly identical to that of folate-rhodamine, confirming that rhodamine intensity could be used as a measure of conjugate concentration *in vivo*.

Finally, the binding affinity of each folate-PEG-rhodamine conjugate for FR on KB cells was analyzed by measuring KB cell fluorescence as a function of conjugate concentration (Figure 2A). While the K_d of folate-rhodamine for FR on cancer cells was found to be ~24 nM, attachment of PEG(5000) increased this K_d to ~70 nM, and linkage of the folate-rhodamine anchor to PEG(20 000) further lowered the affinity to ~185 nM. Conjugation of PEG(60 000), however, caused no further reduction in binding affinity (K_d~187 nM). Although these differences in affinity will have to be considered in our subsequent analysis of the data, it is important to realize that binding of all folate-PEG-rhodamine conjugates was efficiently competed with excess folic acid, demonstrating that all binding was FR mediated (Figure 2A, dotted lines). Moreover, within 30 min of folate-PEG-rhodamine addition, most folate conjugates were endocytosed by their target cells (Supporting Information Figure S3).

Rate of Serum Clearance of Folate-PEG-Rhodamine Conjugates. Because larger sized nanomedicines frequently exhibit longer circulation times *in vivo*, folate-PEG-rhodamine conjugates of different sizes were analyzed for their kinetics of clearance from the blood. The half-life of folate-rhodamine in Balb/c mice was determined to be ~0.5 h, while the larger PEG conjugates had half-lives of 1.2, 3.0, and 9.5 h for folate-PEG(5000)-rhodamine, folate-PEG(20 000)-rhodamine, and folate-PEG(60 000)-rhodamine, respectively (Figure 2B). Thus, folate-PEG-rhodamine conjugates exhibit a circulation half time dependence on size that is similar to other nanoparticles, with the largest increase in area under the curve (AUC) between PEG(20 000) and PEG(60 000); *i.e.*, the approximate molecular weight cutoff for renal filtration.[43] Finally, we also evaluated the stability of the folate-PEG(60 000)-rhodamine conjugate in serum and found the conjugate to remain intact and fluorescent for the duration of the experiment (Figure 2B, dotted line).

Tumor Penetration and Accumulation of Folate-PEG-Rhodamine Conjugates *in Vivo*. Although microscopic evaluation of the perfusion kinetics of drug molecules into malignant masses has been frequently performed on mice containing surgically implanted glass windows over their tumors,[44] we preferred to avoid this model since inflammation associated with surgery can significantly

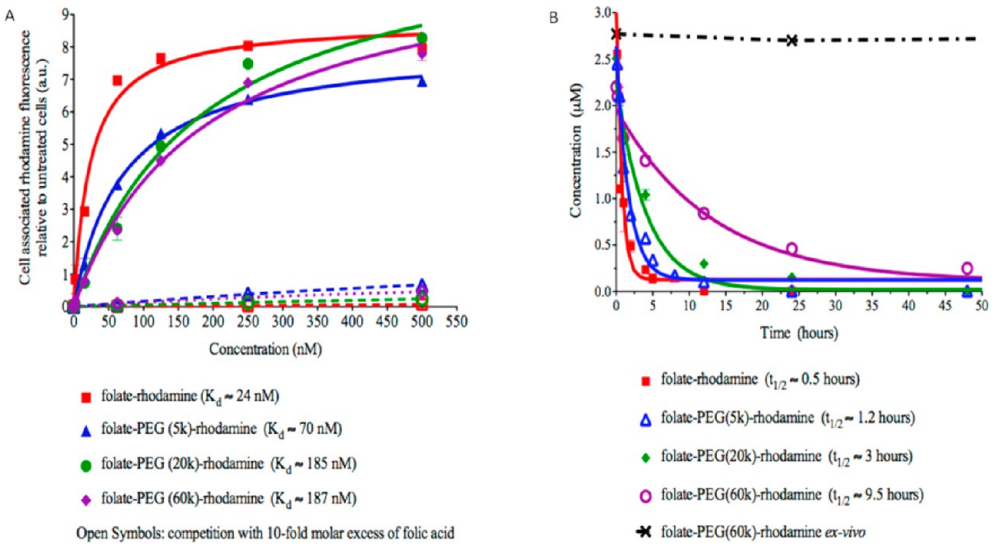

Figure 2. Analysis of folate receptor binding affinity and circulation half-life of folate-PEG-rhodamine conjugates of different PEG sizes. (A) Binding affinities of folate-PEG-rhodamine conjugates to KB cells were determined by incubating the cells with different concentrations of conjugate for 30 min at 4 °C either in the presence (dotted lines) or absence (solid lines) of 10-fold molar excess of free folic acid. After washing to remove unbound conjugate, cells were dissolved in 2% sodium dodecylsulfate, and cell-associated fluorescence was quantitated. (B) Plasma half-lives of folate-PEG-rhodamine conjugates were determined by injecting Balb-c mice i.v. with 500 nmol/kg of each conjugate and analyzing sampled serum for rhodamine fluorescence as described in the Materials and Methods. Dotted line: fresh serum from Balb-c mice was spiked with folate-PEG(60 000)-rhodamine *ex vivo*, and the fluorescence was measured at different time points to determine the conjugate's stability in serum.

influence the permeability of both the vasculature and the tumor. Therefore, in order to monitor the kinetics of tumor penetration of different sized folate-PEG-rhodamine conjugates in a more natural environment, KB tumors were implanted subcutaneously on the legs of athymic nu/nu mice and allowed to grow to ~5−6 mm in diameter. Because the skin covering the tumor was thin, use of multiphoton microscopy enabled visualization of the perfusion and internalization of the targeted fluorescent dyes deep within the tumor masses in a noninvasive manner.

Real time quantitation of tumor concentrations of the larger folate-PEG-rhodamine conjugates following tail vein injection (500 nmol/kg) revealed surprisingly little tumor-associated fluorescence, even at 65 min postadministration (Figure 3A, first row). In order to confirm that this minimal tumor accumulation was not a consequence of insufficient FR or inadequate camera sensitivity, folate-rhodamine was injected into the tail vein of the same mouse at the 65 min time point, and its accumulation was again monitored at the same tumor site. As seen in both the fluorescence micrographs and the associated quantitative plots, folate-rhodamine rapidly penetrated and saturated folate receptors in the same tumor (Figure 3A, second row), maximizing receptor occupancy within ~5 min of conjugate injection. At this 5 min time point, the relative folate-rhodamine uptake was 6 times greater than that seen with the folate-PEG-rhodamine conjugates after 1 h of tumor perfusion. These data suggest that an absence of folate receptors or lack of microscope sensitivity cannot account for the limited accumulation of the folate-PEG-rhodamine conjugates. The data consequently argue that the larger folate-targeted nanoparticles access tumor FR much more slowly than smaller folate-rhodamine conjugate.

More prolonged monitoring of folate-PEG(5000)-rhodamine and folate-PEG(20 000)-rhodamine accumulation in the tumor showed increased but still limited rhodamine fluorescence at 4, 12, and 24 h time points (Figure 4). In contrast, significant accumulation of the same folate-PEG-rhodamine conjugates was prominent in the kidneys by 1.5 h postinjection (Supporting Information Figure S4). Since the kidney constitutes the major nonmalignant tissue known to express FR,[37−39] these data demonstrate that folate-PEG(5000)-rhodamine and folate-PEG(20 000)-rhodamine readily bind FR if they can access the receptor *in vivo*. In fact, the punctate intracellular distribution of the folate-PEG-rhodamine conjugates in the tumor at the 24 h time point strongly suggests that the conjugates were recognized and internalized by FR-mediated endocytosis in the tumor (Figure 4, lower panel). On the basis of these observations, we conclude that the limited tumor accumulation of folate-PEG(5000)-rhodamine and folate-PEG(20 000)-rhodamine conjugates derives from the fact that their excretion by the kidneys is far more rapid than their penetration of the tumors, as suggested by the pharmacokinetic data in Figure 2.

The kinetics of penetration and uptake of folate-PEG(60 000)-rhodamine by the tumor was different

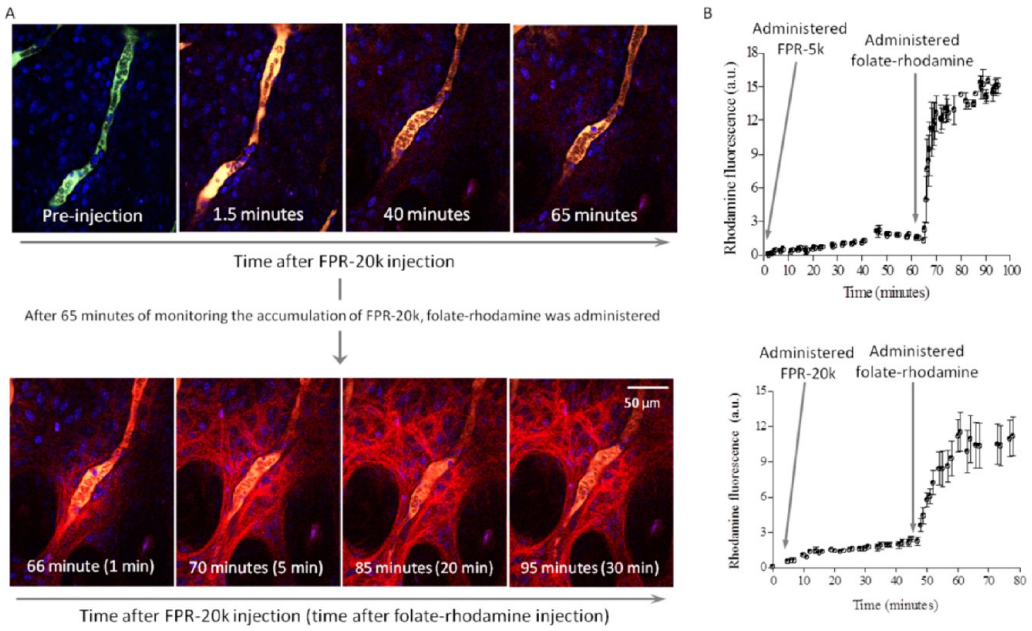

Figure 3. Image analysis of the accumulation of folate-PEG(5000)-rhodamine (FPR-5k) and folate-PEG(20 000)-rhodamine (FPR-20k) in tumor tissue as a function of time following i.v. injection of each conjugate. (A) FPR-20k (red color) was administered i.v. at 500 nmol/kg, and its accumulation in the tumor tissue was monitored for ~65 min (top row), at which time 500 nmol/kg folate-rhodamine (red color) (MW 1069) was injected into the same tail vein, and the uptake of rhodamine was monitored for an additional 30 min (bottom row). (B) Quantitative analysis of the kinetics of accumulation of FPR-5k (top panel) and FPR-20k (bottom panel) in tumor tissue followed by administration of the much smaller folate-rhodamine in the same vein.

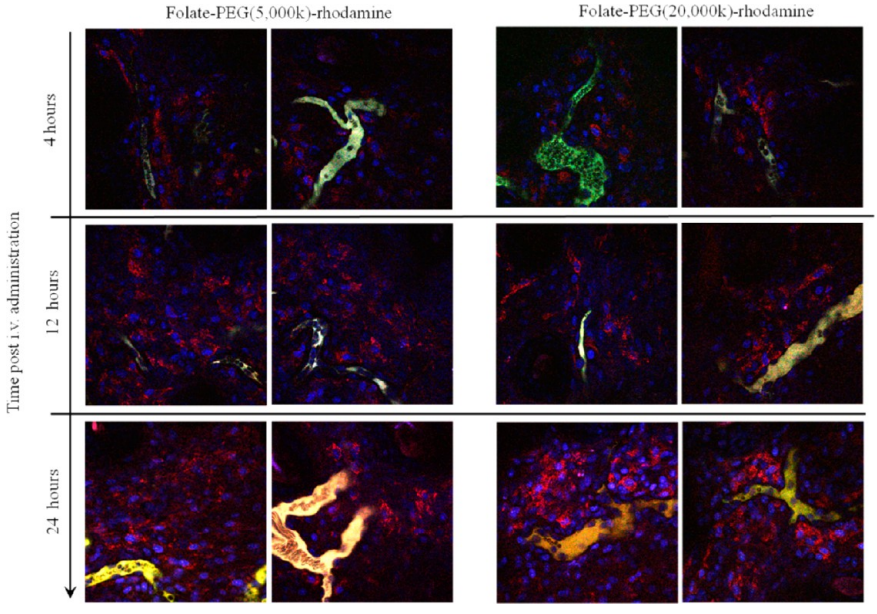

Figure 4. Accumulation of folate-PEG(5000)-rhodamine and folate-PEG(20 000)-rhodamine in tumor tissue at longer time points. 500 nmol/kg of each conjugate (red color) was administered i.v., and tumor uptake was monitored for 24 h. For ease of anatomical analysis, blood vessels were labeled with dextran-FITC (yellow), and cell nuclei were labeled with Hoescht 33342 (blue). The images were taken at random spots around the tumor at a depth ~60−70 μm from the tumor surface.

from folate-PEG(5000)-rhodamine and folate-PEG-(20 000)-rhodamine (Figure 5), with tumor accumulation more prominent at later time points (4−48 h). That this accumulation was, in fact, FR-mediated could be demonstrated by the ability of a 100-fold excess of a water-soluble derivative of folic acid (EC20) to markedly reduce rhodamine fluorescence in the tumor (Supporting Information Figure S5). The strong intracellular punctate distribution of rhodamine fluorescence further confirms this hypothesis (bottom rows). While other explanations are possible, we interpret the more prominent accumulation of folate-PEG(60 000)-rhodamine

in the tumor to arise from the fact that folate-PEG-(60 000)-rhodamine remains in circulation much longer (see Figure 2B), allowing it greater opportunity to perfuse the tumor before it filters through the kidneys. Indeed, accumulation of folate-PEG(60 000)-rhodamine in the tumor was still increasing at the 48 h time point, a property not shared by the smaller folate-rhodamine conjugates.

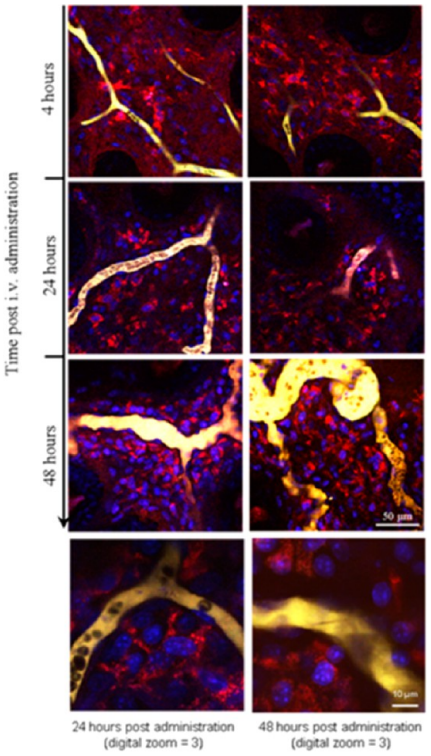

Figure 5. Accumulation of folate-PEG(60 000)-rhodamine at long time points. 500 nmol/kg of the conjugate (red color) was administered i.v. in the tail vein. Tumor-associated rhodamine fluorescence was visualized at 4 h (first row), 24 h (second row), and 48 h (third row). The digital zoom of tumor cells at 24 (left) and 48 h (right) after conjugate administration (bottom row) reveal the intracellular location of the conjugate. For ease of anatomical analysis, blood vessels were labeled with dextran-FITC (yellow), and cell nuclei were labeled with Hoescht 33342 (blue). The images were taken at random spots around the tumor at a depth ~60−70 μm from the tumor surface.

Although the intravenously injected dose of folate-rhodamine (500 nmol/kg) was more than sufficient to saturate all FR in the tumor mass,[36] because of the larger folate-PEG-rhodamine conjugates' lower affinities for FR, we wondered whether a higher dose of folate-PEG-rhodamine might lead to more complete tumor saturation. To test this hypothesis, we repeated the above studies, only we injected 8-fold more folate-PEG(60 000)-rhodamine (*i.e.*, 4000 nmol/kg) to compensate for its 8-fold weaker FR affinity. As shown in Figure 6A and B, this higher dose indeed increased overall tumor-associated fluorescence, but still failed to saturate the tumor, yielding a fluorescence intensity at the 1 h time point that was less than 1/3 the intensity of the saturating dose of folate-rhodamine at a 5 min time point (compare Figure 3B). Because of difficulties associated with keeping these mice alive for extended periods under anesthesia, it was not possible to determine whether folate-PEG(60 000)-rhodamine might eventually saturate tumor FR at very long time points (Figure 6B), but we anticipate that both tumor accumulation and kidney excretion would have continued with similar kinetics.

Comparison of Tumor Accumulation of Folate-BSA-Fluorescein *versus* Folate-Fluorescein. In order to confirm the observed effects of targeted particle size on tumor accumulation in an orthogonal system, we compared accumulation of folate-fluorescein with folate-BSA-fluorescein in the same murine tumor model. At 2 h following tail vein injection of either conjugate, tumors were imaged and then digested, and derived cells were examined for accumulation of folate-fluorescein and folate-BSA-fluorescein by flow cytometry. As seen in Figure 7B, unfractionated cells isolated from tumors from mice not treated with any folate conjugate showed 1% positive cells (negative control). In contrast, cells isolated from tumors of mice injected with folate-fluorescein displayed 15% positive cells, while

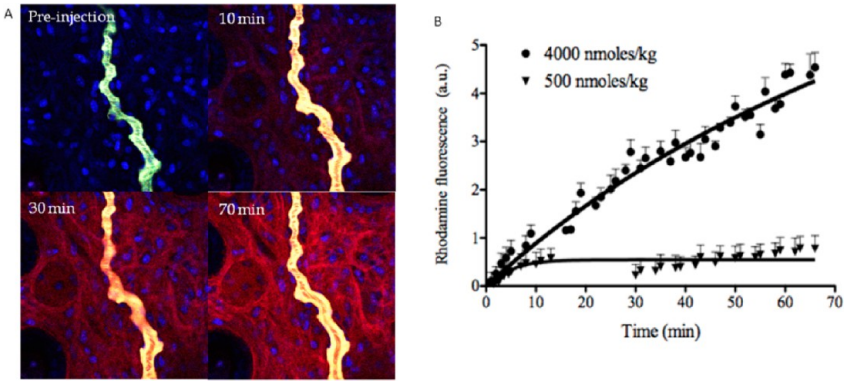

Figure 6. Accumulation of higher doses of folate-PEG(60 000)-rhodamine in tumor tissue as a function of time. (A) 4000 nmol/kg of folate-PEG(60 000)-rhodamine conjugate (red color) was administered i.v., and tumor accumulation was monitored for ~70 min. (B) Comparison of the rates of tumor uptake of folate-PEG(60 000)-rhodamine following i.v. administration of 4000 *versus* 500 nmol/kg of the conjugate.

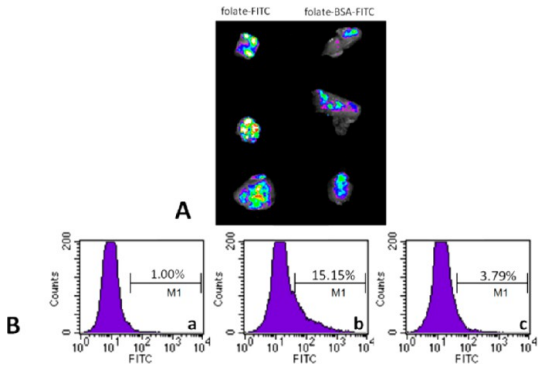

Figure 7. Accumulation of folate-BSA-fluorescein in tumor tissue. (A) Fluorescence images of excised tumors after i.v. administration of 10 nmol of folate-fluorescein (left column) or 10 nmol of folate-BSA-fluorescein (right column). (B) Analysis of fluorescein-labeled cells following collagenase-digestion of solid tumor tissue. Mice were injected intravenously with (a) PBS, (b) 10 nmol of folate-fluorescein, or (c) 10 nmol of folate-BSA-fluorescein and euthanized 2 h later. Tumors were then resected amd digested, and the unfractionated mixture of tumor and stromal cells was analyzed immediately by flow cytometry.

cells from mice injected with folate-BSA-fluorescein yielded only 3.8% labeled cells. After adjusting for the fact that each BSA was conjugated to 7−12 mol of fluorescein (see Materials and Methods), one can estimate that the smaller folate-fluorescein conjugate had accumulated in the tumor mass by the two hour time point ~40-fold more readily on a molar basis than folate-BSA-fluorescein.

One of the anticipated consequences of using ligands to target nanoparticles to pathologic cells in diseased tissues is the emergence of a "binding site barrier", where docking of the initial ligand-targeted nanoparticles to cancer cells most proximal to the blood vessel blocks passage of subsequent nanoparticles to sites deeper in the tumor mass.[45−47] Although the function of this paper was not to quantitate the magnitude of the binding site barrier that impedes tumor perfusion of folate-PEG-rhodamine conjugates, analysis of the images in Figures 4 and 5 reveals that most of the fluorescence is concentrated near a blood vessel. Indeed, a detailed mathematical evaluation of the same data has revealed that the conjugates generate a substantial and sustained binding site barrier that renders their penetration into tumors much slower than that of folate-rhodamine.[48] It will now be important to determine which adjustments in nanoparticle size, shape and/or chemistry can eliminate such impediments while maintaining the desirable drug delivery capabilities of larger nanocarriers.

CONCLUSIONS

Using a well-characterized homologous series of folate-targeted PEG-rhodamine conjugates of different sizes, we have investigated the impact of size on the kinetics of ligand-targeted nanoparticle accumulation in solid tumors *in vivo*. We find that folate-PEG-rhodamine conjugates accumulate more slowly and less efficiently in tumor masses than the much smaller folate-rhodamine conjugate. We also observe that the intermediate sized folate-PEG(5000)-rhodamine and folate-PEG(20 000)-rhodamine achieve only limited tumor accumulation at longer time points, probably because they filter into the urine before they have time to perfuse the tumor. In contrast, the larger folate-PEG(60 000)-rhodamine conjugate may display enhanced tumor cell uptake due to its significantly longer circulation time *in vivo*. The fact that folate targeting augments tumor accumulation of all of the above conjugates can be established from the reduced tumor accumulation of the same conjugates in mice pretreated with excess folate (*i.e.*, to preblock tumor FR) and from the punctate intracellular distributions of the nanoparticles in the tumor cells *in vivo*, suggesting endosomal localization.

Although fewer rhodamine molecules may ultimately be delivered to tumor FR with folate-derivatized nanocarriers, several well characterized merits of nanocarriers can be exploited to at least partially offset their lower tumor accumulation. First, the binding affinity of the nanoparticle for tumor FR can be enhanced by increasing the number of targeting ligands attached to each nanocarrier. Thus, multivalent attachments can augment binding avidity when high affinity monovalent interactions cannot be achieved. Second, the folate-targeted nanoparticles can be loaded with large drug payloads to mitigate their reduced accumulation in tumor sites. Third, higher concentrations of the nanomedicines can be administered to drive greater tumor accumulation as shown in Figure 6. While a variety of other remedies for reduced tumor penetration undoubtedly exist, the final choice of nanoparticle size, shape, chemistry, and targeting ligand will have to be carefully evaluated to ensure optimal performance of each nanocarrier.

MATERIALS AND METHODS

Materials. Fmoc-protected amino acid derivatives, Fmoc-Lys(Mtt)-loaded Wang resin, 2-(1*H*-benzotriazol-1-yl)-1,1,3,3-tetramethyluronium hexafluorophosphate (HBTU), and *N*-hydroxybenzotriazole (HOBT) were purchased from Novabiochem (San Diego, CA). N^{10}-Trifluoroacetylpteroic acid was synthesized from folic acid as described previously.[40] Rhodamine B isothiocyanate, all protein standards, Sephadex G-50 columns, bovine serum albumin-fluorescein (BSA-fluorescein, A9771), 1-ethyl-3-(3-dimethylaminopropyl) carbodiimide (EDC), and blue dextran were all purchased from Sigma (St. Louis, MO). Activated polyetheleneglycol molecules of different molecular weights were obtained from Nektar Therapeutics (San Carlos, CA). Folate-deficient RPMI 1640 medium was obtained from Gibco

BRL (Gaithersburg, MD), and folate-fluorescein was a generous gift from Endocyte, Inc. (West Lafayette, IN). Balb-c mice, athymic nude mice, and folate-deficient rodent chow were purchased from Harlan (Indianapolis, IN). The sources of other chemicals are described in the text.

Synthesis of Folate-PEG-Rhodamine Constructs of Different Sizes. Folate-rhodamine (MW 1069) was synthesized as previously described.[36] Folate-PEG-rhodamine conjugates of larger sizes were assembled in two steps. A folate-rhodamine-SH "anchor" was initially synthesized using standard Fmoc solid phase peptide synthesis on an α-Fmoc-protected lysine-loaded Wang resin as shown in Scheme 1. The folate-rhodamine-SH anchor was then conjugated to a maleimide-activated PEG molecule of the desired size (PEG(5000), PEG(20 000), or PEG(60 000)) as depicted in Scheme 2. The folate-PEG-rhodamine conjugates were purified by gel filtration chromatography using a coarse Sephadex G-50 column equilibrated in water (fractionation range for globular proteins: 1500−30 000) under gravity (Supporting Information Figure S1).

Characterization of the Molecular Weight of Folate-PEG-Rhodamine Conjugates. The apparent molecular weight of each folate-PEG-rhodamine conjugate was determined at room temperature in phosphate buffered saline by gel filtration chromatography on a Sephacryl 100-HR or 200-HR column. The ratio of the elution volume to void volume (V_e/V_o) of each conjugate was compared with the V_e/V_o ratio of protein standards to assess conjugate size. Column void volume was determined by monitoring the elution of blue dextran (M_r ∼2 000 000) at 610 nm, and elution volumes of protein standards were assessed by following absorbance at 280 nm. The 24 cm × 1.0 cm Sephacryl 100-HR column (M_r range 1000−10 000 Da) was used to determine the size of the folate-PEG(5000)-rhodamine conjugate, with bradykinin fragment 2−9 (M_r ∼904), aprotinin from bovine lung (M_r 6511.44), myoglobin from horse heart (M_r ∼17 000), carbonic anhydrase from bovine erythrocytes (M_r ∼29 000), bovine serum albumin (M_r ∼66 000), and aldolase (M_r ∼161 000) used as standards. The 22 cm × 1.0 cm Sephacryl 200-HR (M_r range 5−250 kDa) was employed for assessment of the sizes of the folate-PEG(20 000)-rhodamine and folate-PEG(60 000)-rhodamine conjugates, with myoglobin from horse heart (M_r ∼17 000), carbonic anhydrase (M_r ∼29 000), bovine serum albumin (M_r ∼66 000), alcohol dehydrogenase from yeast (M_r ∼150 000), β-amylase from sweet potato (M_r ∼200 000), apoferritin from horse spleen (M_r ∼443 000), and bovine thyroglobulin (M_r ∼669 000) used as standards.

Characterization of Folate to Rhodamine Ratio for Folate-PEG-Rhodamine Conjugates. To quantitate the ratio of folate to rhodamine on the folate-PEG-rhodamine conjugates, the extinction coefficients of pure folic acid and pure rhodamine B isothiocyanate in water were measured at two different wavelengths, 280 and 560 nm, by constructing standard curves at both wavelengths. Known weights of each folate-PEG-rhodamine conjugate were then dissolved in water, and their absorbances were measured at 280 and 560 nm. The ratio of folate to rhodamine on each targeted conjugate was then determined by solving the simultaneous equations for the concentration of folic acid [FA] and the concentration of rhodamine [Rhod]:

$$A_{280} = \varepsilon_{280}(\text{FA}) \cdot [\text{FA}] + \varepsilon_{280}(\text{Rhod}) \cdot [\text{Rhod}]$$

$$A_{560} = \varepsilon_{560}(\text{FA}) \cdot [\text{FA}] + \varepsilon_{560}(\text{Rhod}) \cdot [\text{Rhod}]$$

***In Vitro* Specific Binding of Folate-PEG-Rhodamine Conjugates.** KB cells (a FR-positive malignant human cancer cell line) were obtained from American Type Culture Collection (Rockville, MD) and cultured at 37 °C in a humidified atmosphere containing 5% CO_2. The cells were grown continuously as a monolayer in folate-deficient RPMI 1640 medium supplemented with 10% fetal bovine serum, penicillin (50 units/mL), and streptomycin (50 μg/mL). To establish the specificity of folate conjugate binding, 10^6 KB cells were suspended in 1 mL of folate-deficient RPMI 1640 medium and incubated with 100 nM of a folate-PEG-rhodamine conjugate for 30 min at 37 °C in the presence or absence of excess competing ligand (100-fold molar excess of free folic acid, preincubation for 5 min). After incubation, the cells were washed 3 times with ice-cold PBS and resuspended in PBS. Cells were then examined under a fluorescent microscope (Olympus BH-2), and images were taken using an Olympus DP70 digital camera.

Binding Affinity of Folate-PEG-Rhodamine Conjugates. KB cells were seeded into 6-well plates and grown until they reached ∼90% confluence. The cells were then incubated at 4 °C with different concentrations of the desired folate-PEG-rhodamine conjugate either in the presence or absence of a 10-fold excess of folic acid for 30 min at 37 °C. After incubation the cells were washed 3 times in ice-cold PBS, and 2 mL of 2% SDS solution was added to each well to dissolve the cells. Rhodamine fluorescence was measured in each cell solution using an AMINCO Bowman Series 2 luminescence spectrometer (SLM Instruments).

Analysis of Rate of Clearance of Folate-PEG-Rhodamine Conjugates from Circulation. Animal procedures were carried out with approval of the Purdue Animal Care and Use Committee. Mice were injected intravenously with 500 nmol/kg of folate-PEG-rhodamine conjugate, and ∼200−300 μL of blood was collected at the desired times over the next 48 h *via* paraorbital bleeding. After allowing 1−2 h for the blood to coagulate, the serum was collected and analyzed for rhodamine fluorescence. A standard curve of rhodamine fluorescence intensity in Balb-c serum *versus* concentration was constructed for each conjugate and used to estimate the concentration of each folate-PEG-rhodamine conjugate in each serum sample. The circulation half-life for each conjugate was approximated by plotting the intensity of rhodamine fluorescence in the serum *versus* time.

***In Vivo* Uptake and Accumulation of Folate-PEG-Rhodamine Conjugates.** Real-time tumor accumulation of each folate-PEG-rhodamine conjugate was monitored using two-photon microscopy and analyzed as described previously.[36]

***In Vivo* Uptake and Accumulation of Folate-BSA-Fluorescein.** Folate-BSA-fluorescein was synthesized and characterized as previously described.[41] Female athymic nude mice were implanted subcutaneously with 10^6 KB cells, and after allowing 3 weeks for tumors to grow, mice were injected *via* tail vein with 10 nmol of either folate-fluorescein or folate-BSA-fluorescein. After 2 h, mice were euthanized and imaged using a Kodak Image Station operated with Kodak molecular imaging software (version 4.5; Carestream Molecular Imaging). Fluorescent image settings were as follows: illumination source = multiwavelength, acquisition time = 2 min, f-stop = 2.8, focal plane = 5, FOV = 160, binning = 2 × 2, excitation filter = 465 nm, emission filter = 535 nm. White light image settings were as follows: illumination source = white light transillumination, acquisition time = 0.175 s, f-stop = 11, focal plane = 5, FOV = 160, binning = none, excitation = white light, emission filter = none. After image acquisition, tumors were resected and digested for 1 h with a cocktail containing 10 mg of collagenase, 1 mg of hyaluronidase, and 0.2 mg of deoxyribonuclease 1 in 10 mL of folate deficient media and then filtered through a 40 μm cell strainer and analyzed on a FACSCalibur flow cytometer (BD Bioscience) with CellQuant software version 3.5.

Conflict of Interest: The authors declare the following competing financial interest(s): P.S.L. has received fees and stock from Endocyte Inc. (West Lafayette, IN, USA), a company that he cofounded in 1995 to develop treatments for cancer and inflammation. All other authors declare no competing interests.

Acknowledgment. Thank you to Robert A. Reason for creating the Table of Contents graphic and to Christopher Galliford for helping to edit the paper. This work was supported by a grant from Endocyte, Inc.

Supporting Information Available: Additional characterization of folate-PEG-rhodamine conjugates, *in vivo* up-take in various organs, and *in vivo* competition studies. This material is available free of charge *via* the Internet at http://pubs.acs.org.

REFERENCES AND NOTES

1. Dreher, M. R.; Liu, W.; Michelich, C. R.; Dewhirst, M. W.; Yuan, F.; Chilkoti, A. Tumor Vascular Permeability, Accumulation, and Penetration of Macromolecular Drug Carriers. *J. Natl. Cancer Inst.* **2006**, *98*, 335–344.

2. Torchilin, V. P. Recent Advances with Liposomes as Pharmaceutical Carriers. *Nat. Rev. Drug Discovery* **2005**, *4*, 145–160.
3. Kataoka, K.; Harada, A.; Nagasaki, Y. Block Copolymer Micelles for Drug Delivery: Design, Characterization and Biological Significance. *Adv. Drug Delivery Rev.* **2001**, *47*, 113–131.
4. Senter, P. D.; Springer, C. J. Selective Activation of Anticancer Prodrugs by Monoclonal Antibody-Enzyme Conjugates. *Adv. Drug Delivery Rev.* **2001**, *53*, 247–264.
5. Patri, A. K.; Majoros, I. J.; Baker, J. P. Dendritic Polymer Macromolecular Carriers for Drug Delivery. *Curr. Opin. Chem. Biol.* **2002**, *6*, 466–471.
6. Jones, M. C.; Leroux, J. C. Polymeric Micelles—A New Generation of Colloidal Drug Carriers. *Eur. J. Pharm. Biopharm.* **1999**, *48*, 101–111.
7. Panyam, J.; Labhasetwar, V. Biodegradable Nanoparticles for Drug and Gene Delivery to Cells and Tissue. *Adv. Drug Delivery Rev.* **2003**, *55*, 329–347.
8. Muller, R. H.; Mader, K.; Gohla, S. Solid Lipid Nanoparticles (SLN) for Controlled Drug Delivery—A Review of the State of the Art. *Eur. J. Pharm. Biopharm.* **2000**, *50*, 161–177.
9. De Jong, W. H.; Borm, P. J. A. Drug Delivery and Nanoparticles: Applications and Hazards. *Int. J. Nanomed.* **2008**, *3*, 133–149.
10. Wang, A. Z.; Langer, R.; Farokhzad, O. C. Nanoparticle Delivery of Cancer Drugs. *Annu. Rev. Med.* **2012**, *63*, 185–198.
11. Matsumura, Y.; Maeda, H. A New Concept for Macromolecular Therapeutics in Cancer Chemotherapy: Mechanism of Tumoritropic Accumulation of Proteins and the Antitumor Agent Smancs. *Cancer Res.* **1986**, *46*, 6387–6392.
12. Maeda, H.; Matsumura, Y. Tumoritropic and Lymphotropic Principles of Macromolecular Drugs. *Crit. Rev. Ther. Drug Carrier Syst.* **1989**, *6*, 193–210.
13. Maeda, H.; Seymour, L. W.; Miyamoto, Y. Conjugates of Anticancer Agents and Polymers: Advantages of Macromolecular Therapeutics *in Vivo*. *Bioconjugate Chem.* **1992**, *3*, 351–362.
14. Masubuchi, N. Pharmacokinetics of DE-310, a Novel Macromolecular Carrier System for the Camptothecin Analog DX-8951f, in Tumor-Bearing Mice. *Pharmazie* **2004**, *59*, 374–377.
15. Mori, A.; Klibanov, A. L.; Torchilin, V. P.; Huang, L. Influence of the Steric Barrier Activity of Amphipathic Poly(ethyleneglycol) and Ganglioside GM1 on the Circulation Time of Liposomes and on the Target Binding of Immunoliposomes *in Vivo*. *FEBS Lett.* **1991**, *284*, 263–266.
16. Kaneda, Y.; Tsutsumi, Y.; Yoshioka, Y.; Kamada, H.; Yamamoto, Y.; Kodaira, H.; Tsunoda, S.; Okamoto, T.; Mukai, Y.; Shibata, H.; *et al.* The Use of PVP as a Polymeric Carrier to Improve the Plasma Half-Life of Drugs. *Biomaterials* **2004**, *25*, 3259–3266.
17. Dvorak, H. F.; Nagy, J. A.; Dvorak, J. T.; Dvorak, A. M. Identification and Characterization of the Blood Vessels of Solid Tumors that are Leaky to Circulating Macromolecules. *Am. J. Pathol.* **1988**, *133*, 95–109.
18. Jain, R. K.; Baxter, L. T. Mechanisms of Heterogeneous Distribution of Monoclonal Antibodies and Other Macromolecules in Tumors: Significance of Elevated Interstitial Pressure. *Cancer Res.* **1988**, *48*, 7022–7032.
19. Jang, S. H.; Wientjes, M. G.; Lu, D.; Au, J. L-S. Drug Delivery and Transport to Solid Tumors. *Pharm. Res.* **2003**, *20*, 1337–1350.
20. Wang, J.; Lu, Z.; Gao, Y.; Wientjes, M. G.; Au, J. L-S. Improving Delivery and Efficacy of Nanomedicines in Solid Tumors. *Nanomedicine* **2011**, *6*, 1605–1620.
21. Ross, J. S.; Schenkein, D, P.; Pietrusko, R.; Rolfe, M.; Linette, G. P.; Stec, J.; Stagliano, N. E.; Ginsburg, G. S.; Symmans, W. F.; Pusztai, L.; *et al.* Targeted Therapies for Cancer 2004. *Am. J. Clin. Pathol.* **2004**, *122*, 598–609.
22. Allen, T. M. Ligand-Targeted Therapeutics in Anticancer Therapy. *Nat. Rev. Cancer* **2002**, *2*, 750–763.
23. Singh, R.; Lillard, J. W., Jr. Nanoparticle-Based Targeted Drug Delivery. *Exp. Mol. Pathol.* **2009**, *86*, 215–223.
24. Ganta, S.; Devalapally, H.; Shahiwala, A.; Amiji, M. A Review of Stimuli-Responsive Nanocarriers for Drug and Gene Delivery. *J. Controlled Release* **2008**, *126*, 187–204.
25. Cheng, Z.; Zaki, A. A.; Hui, J. Z.; Muzykantov, V. R.; Tsourkas, A. Multifunctional Nanoparticles: Cost *versus* Benefit of Adding Targeting and Imaging Capabilities. *Science* **2012**, *338*, 903–910.
26. Gu, F. X.; Karnik, R.; Wang, A. Z.; Alexis, F.; Levy-Nissenbaum, E.; Hong, S.; Langer, R. S.; Farokhzad, O. C. Targeted Nanoparticles for Cancer Therapy. *Nanotoday* **2007**, *2*, 14–21.
27. Gupta, Y.; Jain, A.; Jain, P.; Jain, S. K. Design and Development of Folate Appended Liposomes for Enhanced Delivery of 5-fu to Tumor Cells. *J. Drug Targeting* **2007**, *15*, 231–240.
28. Stevens, P. J.; Sekido, M.; Lee, R. J. A Folate Receptor-Targeted Lipid Nanoparticle Formulation for a Lipophilic Paclitaxel Prodrug. *Pharm. Res.* **2004**, *21*, 2153–2157.
29. Pan, X. Q.; Wang, H.; Lee, R. J. Antitumor Activity of Folate Receptor Targeted Liposomal Doxorubicin in a KB Oral Carcinoma Murine Xenograft Model. *Pharm. Res.* **2003**, *20*, 417–422.
30. Ohguchi, Y.; Kawano, K.; Hattori, Y.; Maitani, Y. Selective Delivery of Folate-PEG-Linked, Nanoemulsion-Loaded Aclacinomycin A to KB Nasopharyngeal Cells and Xenograft: Effect of Chain Length and Amount of Folate-PEG Linker. *J. Drug Targeting* **2008**, *16*, 660–667.
31. Shiokawa, T.; Hattori, Y.; Kawano, K.; Ohguchi, Y.; Kawakami, H.; Toma, K.; Maitani, Y. Effect of Polyethylene Glycol Linker Chain Length of Folate-Linked Microemulsions Loading Aclacinomycin A on Targeting Ability and Antitumor Effect *in Vitro* and *in Vivo*. *Clin. Cancer Res.* **2005**, *11*, 2018–2025.
32. Fujimori, K.; Covell, D. G.; Fletcher, J. E.; Weinstein, J. N. A Modeling Analysis of Monoclonal Antibody Percolation Through Tumors: a Binding-Site Barrier. *J. Nucl. Med.* **1990**, *31*, 1191–1198.
33. Juweid, M.; Neumann, R.; Paik, C.; Perez-Bacete, M. J.; Sato, J.; van Osdol, W.; Weinstein, J. N. Micropharmacology of Monoclonal Antibodies in Solid Tumors: Direct Experimental Evidence for a Binding Site Barrier. *Cancer Res.* **1992**, *52*, 5144–5153.
34. Saga, T.; Neumann, R. D.; Heya, T.; Sato, J.; Kinuya, S.; Le, N.; Paik, C. H.; Weinstein, J. N. Targeting Cancer Micrometastases with Monoclonal Antibodies: A Binding-Site Barrier. *Proc. Natl. Acad. Sci. U. S. A.* **1995**, *92*, 8999–9003.
35. Graff, C. P.; Wittrup, K. D. Theoretical Analysis of Antibody Targeting of Tumor Spheroids: Importance of Dosage for Penetration, and Affinity for Retention. *Cancer Res.* **2003**, *63*, 1288–1296.
36. Vlashi, E.; Sturgis, J. E.; Thomas, M.; Low, P. S. Real Time, Noninvasive Imaging and Quantitation of the Accumulation of Ligand-Targeted Drugs into Receptor-Expressing Solid Tumors. *Mol. Pharmaceutics* **2009**, *6*, 1868–1875.
37. Weitman, S. D.; Lark, R. H.; Coney, L. R.; Fort, D. W.; Frasca, V.; Zurawski, V. R., Jr.; Kamen, B. A. Distribution of the Folate Receptor GP38 in Normal and Malignant Cell Lines and Tissues. *Cancer Res.* **1992**, *52*, 3396–3401.
38. Ross, J. F.; Chaudhuri, P. K.; Ratnam, M. Differential Regulation of Folate Receptor Isoforms in Normal and Malignant Tissues *in Vivo* and in Established Cell Lines. Physiologic and Clinical Implications. *Cancer* **1994**, *73*, 2432–2443.
39. Parker, N.; Turk, M. J.; Westrick, E.; Lewis, J. D.; Low, P S.; Leamon, C. P. Folate Receptor Expression in Carcinomas and Normal Tissues Determined by a Quantitative Radioligand Binding Assay. *Anal. Biochem.* **2005**, *338*, 284–293.
40. Luo, J.; Smith, M. D.; Lantrip, D. A.; Wang, S.; Fuchs, P. L. Efficient Syntheses of Pyrofolic Acid and Pteroyl Azide, Reagents for the Production of Carboxyl-Differentiated Derivatives of Folic Acid. *J. Am. Chem. Soc.* **1997**, *119*, 10004–10013.
41. Turek, J. J.; Leamon, C. P.; Low, P. S. Endocytosis of Folate-Protein Conjugates: Ultrastructural Localization in KB Cells. *J. Cell Sci.* **1993**, *106*, 423–430.
42. Fee, C. J.; Van Alstine, J. M. Prediction of the Viscosity Radius and the Size Exclusion Chromatography Behavior of PEGylated Proteins. *Bioconjugate Chem.* **2004**, *15*, 1304–1313.

43. Choi, C. H. J.; Zuckerman, J. E.; Webster, P.; Davis, M. E. Targeting Kidney Mesangium by Nanoparticles of Defined Size. *Proc. Natl. Acad. Sci. U. S. A.* **2011**, *108*, 6656–6661.
44. Hak, S.; Reitan, N. K.; Haraldseth, O.; de Lange Davies, C. Intravital Microscopy in Window Chambers: A Unique Tool to Study Tumor Angiogenesis and Delivery of Nanoparticles. *Angiogenesis* **2010**, *13*, 113–130.
45. Jain, R. K. Delivery of Molecular and Cellular Medicine to Solid Tumors. *Adv. Drug Delivery Rev.* **2001**, *46*, 149–168.
46. van Osdol, W.; Fujimori, K.; Weinstein, J. N. An Analysis of Monoclonal Antibody Distribution in Microscopic Tumor Nodules: Consequences of a "Binding Site Barrier". *Cancer Res.* **1991**, *51*, 4776–4784.
47. Weinstein, J. N.; van Osdol, W. Early Intervention in Cancer Using Monoclonal Antibodies and Other Biological Ligands: Micropharmacology and the "Binding Site Barrier". *Cancer Res.* **1992**, *52*, 2747s–2751s.
48. Schuff, M. M.; Vlashi, E.; Low, P. S.; Nauman, E. A. Quantitative evaluation of receptor mediated targeting of solutes in cancerous tissue using a microvascular mixture theory model. *J. Nanotechnol. Eng. Med.*, manuscript submitted.